JOURNAL OF MATERIALS SCIENCE 27 (1992) 3155–3166

Interfacial debonding and fibre pull-out stresses

Part II *A new model based on the fracture mechanics approach*

LI-MIN ZHOU, JANG-KYO KIM, YIU-WING MAI
Centre for Advanced Materials Technology, Department of Mechanical Engineering, University of Sydney, Sydney, New South Wales, 2006, Australia

An improved analysis has been developed for the interfacial debond stress in a fibre pull-out model based on the concept of fracture mechanics where the debonded region is considered as an interfacial crack and its extension is dependent on a fracture energy criterion being satisfied. By evaluating the partial debond stress, σ_d^p against debond length l, during progressive debonding, instability conditions are derived where the maximum debond stress, σ_d^*, is determined for different embedded fibre length, L. Comparisons between theory and experimental fibre pullout results on several composite systems show that the present model gives excellent prediction of the maximum debond stress, σ_d^*, for the whole range of L including even the very short L, whereas the previous Gao–Mai–Cotterell model, also developed on the basis of a fracture mechanics approach, always overestimates σ_d^* for short L and gives a finite value for $L = 0$. The initial frictional pull-out stress, σ_{fr}, after complete debonding predicted by the present model is basically the same as the Gao–Mai–Cotterell model and agrees well with experiments. The implications of stress distributions in the constituents for different composite systems are discussed on the basis of the proposed debond criterion.

1. Introduction

Two typical theories of interfacial debonding and fibre pull-out (Gao *et al.* [2] and Hsueh [3, 4] which have been developed on the basis of fracture mechanics and the shear strength criterion, respectively) were critically compared [1] with experimental results of several composite systems. It is shown that the Gao–Mai–Cotterell model [2] predicts the trend of maximum debond stress, σ_d^*, very well for long embedded length, L, but it always overestimates σ_d^* for very short L, particularly for epoxy-based matrix composites which display more pronounced instability for short L than ceramic-based matrix composites. An explanation for the inadequacy of the model for σ_d^* is that it originally assumes a progressive stable debond crack propagation at a constant frictionless debond stress, σ_0, along an infinitely long L. Further, the stresses and hence the associated elastic strain energy in the constituents at the bonded region have not been considered in the debond analysis of the model. Also neglected is the shear strain energy in the matrix which is an important contribution to the total strain energy [5]. In contrast, Hsueh's model [3, 4] gives good predictions of σ_d^* for short L but it often needs adjustment to the bond (shear) strength to fit the experimental results for long L. This appears to arise mainly from an underestimate of the frictionless debond stress, σ_0, due to an inappropriately defined stress condition at the boundary of the bonded and debonded regions. Therefore, the effect of matrix axial stress existing at the debonded (but frictionally connected) region is completely neglected. With respect to the initial frictional pull-out stress, σ_{fr}, after complete debonding, the agreement between the two theories and experiments is excellent over the whole range of L for all composite systems studied, suggesting that the solutions for σ_{fr} proposed by the two models are essentially identical.

The present study describes an improved interfacial debonding and fibre pull-out model developed on the basis of a fracture mechanics approach where a predebonded interface is treated as a crack propagating along the fibre length with a constant interfacial fracture energy. In the light of the critical comparison between theories and experimental results as summarized above, omissions and assumptions considered to be inadequate in the previous theories are now properly included in the new model. The fibre is assumed to have a precisely cylindrical shape, so that the effects of surface roughness do not arise. The fibre–matrix interface is either perfectly bonded or totally debonded (but being held together by non-uniform friction due to interfacial pressure which arises from matrix shrinkage and Poisson contraction of the fibre subjected to tension). The approximate analysis given in the present model leads to relatively simple closed-form formulae for all basic results, although some of the non-dimensional coefficients turn out to be rather lengthy expressions.

2. Analysis

2.1. Basic governing equations

Following the earlier approach, a simple shear lag model is considered as shown in Fig. 1, where a fibre

0022–2461

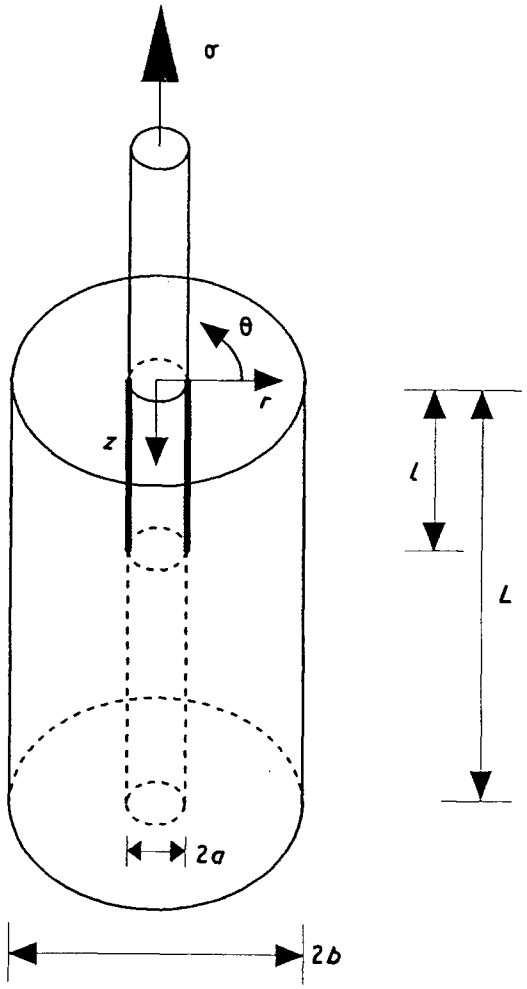

Figure 1 A schematic illustration of the partially debonded fibre in a fibre pull-out model.

(of radius a) is embedded at the centre of a coaxial cylindrical shell of matrix (of an outer radius b) with a volume ratio of the fibre to the matrix $\gamma = a^2/(b^2 - a^2)$. L is the total embedded fibre length with a partial debond region of length, l, from the free fibre-end. In the single-fibre pull-out experiments, the matrix is fixed at one end ($z = L$) and a tensile stress, σ, is applied to the other end ($z = 0$) of the embedded fibre. Shear lag analysis for other boundary conditions with restrained matrix top and fixed matrix and fibre bottom ends are given elsewhere [6]. The external stress, σ, is represented by σ_0, σ_d^p, σ_d^* and σ_{fr} for frictionless (initial) debond stress, partial debond stress, maximum debond stress and initial frictional pull-out stress after complete debonding, respectively, at different stages of the fibre pull-out process.

A set of cylindrical coordinates (r, θ, z) is selected so that the z-axis corresponds to the axis of the fibre. The mode of deformation is axisymmetric and thus the stress components $(\sigma^r, \sigma^\theta, \sigma^z, \tau^{rz})$ and the displacement components (u^r, u^z) are all independent of θ. The remaining stress and displacement components are all zero. For perfectly elastic and isotropic fibre and matrix, the general relation between strains and stresses can be written as

$$\varepsilon_f^z(r, z) = \partial u_f^z/\partial z = (1/E_f)\{\sigma_f^z(r, z) - \nu_f[\sigma_f^r(r, z) + \sigma_f^\theta(r, z)]\} \quad (1)$$

$$\varepsilon_f^\theta(r, z) = u_f^r/r = (1/E_f)\{\sigma_f^\theta(r, z) - \nu_f[\sigma_f^r(r, z) + \sigma_f^z(r, z)]\} \quad (2)$$

for the fibre (i.e. $0 \leqslant r \leqslant a$), and

$$\varepsilon_m^z(r, z) = \partial u_m^z/\partial z = (1/E_m)\{\sigma_m^z(r, z) - \nu_m[\sigma_m^r(r, z) + \sigma_m^\theta(r, z)]\} \quad (3)$$

$$\varepsilon_m^\theta(r, z) = u_m^r/r = (1/E_m)\{\sigma_m^\theta(r, z) - \nu_m[\sigma_m^r(r, z) + \sigma_m^z(r, z)]\} \quad (4)$$

$$\varepsilon_m^{rz}(r, z) = \partial u_m^z/\partial r = [2(1 + \nu_m)/E_m]\tau_m^{rz}(r, z) \quad (5)$$

for the matrix (i.e. $a \leqslant r \leqslant b$), where E and ν are Young's modulus and Poisson's ratio respectively. The subscripts f and m refer to fibre and matrix and the superscripts are coordinate directions. In Equation 5 for the matrix shear strain, the radial displacement gradient with respect to the z-direction is neglected as compared with the axial displacement gradient with respect to the r-direction. Further, assuming to a first approximation that a plane normal to the z-direction remains plane in plane strain deformation, the axial stress in the matrix may be taken as the average of the matrix stresses in the r-direction [2], i.e.

$$\sigma_m^z(z) = [2/(b^2 - a^2)]\int_a^b \sigma_m^z(r, z)r\,dr \quad (6)$$

This assumption is considered appropriate for the model cylindrical composite having a fibre embedded in a relatively large matrix as in a practical fibre pull-out experiment. It is expected in reality, that the variation of the axial matrix stress with regard to the radial direction is substantial only near the fibre free end (or near the debond crack tip for partial debonding) where all stress components are concentrated, but it diminishes with distance away from this region. In fact, with this assumption, several investigators [7, 8] have successfully presented Lame solutions to predict the matrix axial deformation which compare favourably with results from an accurate numerical analysis. Even in a more exact thermo-mechanics model proposed recently by McCartney [9], an average value has been introduced for the axial matrix stress which is necessary to satisfy the remaining equilibrium equations and boundary conditions. Therefore, the mechanical equilibrium condition between the external applied stress and the internal stress distribution requires that

$$\sigma = \sigma_f^z(z) + (1/\gamma)\sigma_m^z(z) \quad (7)$$

The internal stress is transferred from the fibre to the surrounding matrix through the interfacial shear stress $\tau_i^{rz}(z)$. Equilibrium between these stresses is described by

$$\frac{d\sigma_f^z(z)}{dz} = -\frac{2}{a}\tau_i^{rz}(z) \quad (8)$$

2.2. Solution for the stress components in the bonded region ($l \leqslant z \leqslant L$)

The solutions for the axial and shear stresses in the constituents are obtained with given boundary conditions in Appendix 1 as

$$\sigma_f^z(z) = \left\{\frac{[(A_2/A_1)\sigma + \sigma_l]\sinh[A_1^{1/2}(L - z)] - (A_2/A_1)\sigma \sinh[A_1^{1/2}(l - z)]}{\sinh[A_1^{1/2}(L - l)]}\right\} - (A_2/A_1)\sigma \quad (9)$$

$$\sigma_m^z(z) = -\gamma\left\{\frac{[(A_2/A_1)\sigma + \sigma_l]\sinh[A_1^{1/2}(L - z)] - (A_2/A_1)\sigma \sinh[A_1^{1/2}(l - z)]}{\sinh[A_1^{1/2}(L - l)]}\right\} + \gamma(1 + A_2/A_1)\sigma \quad (10)$$

$$\tau_m^{rz}(r, z) = \gamma A_1^{1/2}[(b^2 - r^2)/2r] \times\left\{\frac{[(A_2/A_1)\sigma + \sigma_l]\cosh[A_1^{1/2}(L - z)] - (A_2/A_1)\sigma \cosh[A_1^{1/2}(l - z)]}{\sinh[A_1^{1/2}(L - l)]}\right\} \quad (11)$$

$$\tau_i^{rz}(z) = \frac{a A_1^{1/2}}{2}\left\{\frac{[(A_2/A_1)\sigma + \sigma_l]\cosh[A_1^{1/2}(L - z)] - (A_2/A_1)\sigma \cosh[A_1^{1/2}(l - z)]}{\sinh[A_1^{1/2}(L - l)]}\right\} \quad (12)$$

where

$$A_1 = \frac{2[\alpha(1 - 2k\nu_f) + \gamma(1 - 2k\nu_m)]}{(1 + \nu_m)[2\gamma b^2 \ln(b/a) - a^2]} \quad (13)$$

$$A_2/A_1 = \frac{-\gamma(1 - 2k\nu_m)}{\alpha(1 - 2k\nu_f) + \gamma(1 - 2k\nu_m)} \approx \frac{-\gamma}{\alpha + \gamma} \quad (14)$$

$k = (\alpha\nu_f + \gamma\nu_m)/[\alpha(1 - \nu_f) + 1 + \nu_m + 2\gamma]$ and $\alpha = E_m/E_f$ which is the Young's modulus ratio of the matrix to the fibre. σ_l is defined as the crack tip debond stress acting at the boundary between bonded and debonded regions $z = l$.

2.3. Solution for the stress components in the debonded region ($0 \leqslant z \leqslant l$)

In the debonded region ($0 \leqslant z \leqslant l$), frictional slip occurs at the interface where the stress transfer is governed by the Coulomb friction law. Assuming a constant coefficient of friction, μ, along the debonded interface, it follows that

$$\tau_i^{rz}(z) = -\mu[q_0 + q^*(z)] \quad (15)$$

where q_0 is the residual clamping stress (compressive) caused by the matrix shrinkage and differential thermal contraction (or expansion) of the constituents occurring during fabrication of the composite and $q^*(z)$ is the additional radial stress at the interface arising from Poisson contraction of the fibre which is subjected to tension as given in Equation A5. Further, Gao *et al.* [2] provides the solution for the axial stresses in the fibre and the matrix at the debonded region as

$$\sigma_f^z(z) = \sigma - \omega(\bar{\sigma} - \sigma)[\exp(\lambda z) - 1] \quad (16)$$

$$\sigma_m^z(z) = \gamma\omega(\bar{\sigma} - \sigma)[\exp(\lambda z) - 1] \quad (17)$$

where λ is the reciprocal length giving the effective frictional shear stress transfer and $\bar{\sigma}$ is the asymptotic debond stress for long embedded length. These parameters are related to the interfacial properties as

$$\lambda = 2\mu k/a \quad (18)$$

$$\bar{\sigma} = -q_0/\omega k \quad (19)$$

where $\omega = \alpha\nu_f/(\alpha\nu_f + \gamma\nu_m)$. Combining Equations 16 and 17 with Equations 8 and A3, solutions for the shear stresses in the matrix and at the interface are obtained

$$\tau_m^{rz}(r, z) = [\gamma\lambda\omega(b^2 - r^2)/2r](\bar{\sigma} - \sigma)\exp(\lambda z) \quad (20)$$

$$\tau_i^{rz}(z) = (a\lambda\omega/2)(\bar{\sigma} - \sigma)\exp(\lambda z) \quad (21)$$

2.4. Fibre–matrix debond criterion and solution for the external applied stress

To derive an interfacial debond criterion the concept of fracture mechanics is used such that the differential elastic strain energy stored in the constituents with respect to the incremental debond length is equated to the interfacial fracture toughness, G_{ic} (or specific work of fracture of the interface) [2], i.e.

$$G_{ic} = (1/2\pi a)\frac{\partial U_t}{\partial l} \quad (22)$$

where U_t is the sum of the elastic strain energy stored in the bonded region (U_b, for $l \leqslant z \leqslant L$) and debonded region ($U_d$, for $0 \leqslant z \leqslant l$) which can be obtained by integrating the stress components acting in the constituents over the volume of respective regions

$$\begin{aligned} U_t &= U_b + U_d \\ &= \int_l^L\int_0^a \frac{\sigma_f(z)^2}{E_f}\pi r dr dz + \int_l^L\int_a^b\left[\frac{\sigma_m(z)^2}{E_m} + \frac{2(1 + \nu_m)\tau_m(r, z)^2}{E_m}\right]\pi r dr dz \\ &\quad + \int_0^l\int_0^a \frac{\sigma_f(z)^2}{E_f}\pi r dr dz + \int_0^l\int_a^b\left[\frac{\sigma_m(z)^2}{E_m} + \frac{2(1 + \nu_m)\tau_m(r, z)^2}{E_m}\right]\pi r dr dz \end{aligned} \quad (23)$$

It has been pointed out [10] that Piggott [5] incorrectly derived a debond criterion by equating the

total elastic strain energy (for fibre axial and matrix shear deformation in the bonded region) directly to the interfacial fracture energy, which is certainly not an appropriate fracture mechanics approach. Later, Penn and Lee [11] correctly took the energy balance equation in a differential form, though using the stress equations given by Piggott [5].

Substituting the solutions for the three major stress components determined in the bonded and debonded regions as given in Equations 9–11, 16, 17 and 20 into Equation 22, a debond criterion is derived as

$$2\pi a G_{ic} = B\sigma^2 + C(\bar{\sigma} - \sigma)\sigma + D(\bar{\sigma} - \sigma)^2 \quad (24)$$

where the coefficients B, C and D are complex functions of material properties of the constituents and geometric factors including the radii of the constituents a and b, and the debond length, l, relative to the total embedded fibre length, L. Further details are given in Appendix 2. Therefore, rearrangement of Equation 24 gives the final solution for the external applied stress, σ, as

$$\sigma = \left[\frac{2\pi a G_{ic}}{B - C + D} + \frac{C^2 - 4BD}{4(B - C + D)^2}\bar{\sigma}^2\right]^{1/2} + \frac{2D - C}{2(B - C + D)}\bar{\sigma} \quad (25)$$

As mentioned earlier, the external stress σ, in Equation 25 represents the frictionless (initial) debond stress, σ_0, partial debond stress, σ_d^p, maximum debond stress, σ_d^*, and initial frictional pull-out stress, σ_{fr}, after complete debonding at different stages of the fibre pull-out process depending on the instantaneous debond length, l.

The partial debond stress, σ_d^p, during progressive debonding may be written as a function of the debond length, l, and the crack tip debond stress, σ_l, of Equation A7 which is the axial fibre stress acting at the boundary between bonded and debonded regions $z = l$. Thus

$$\sigma_d^p = \sigma_l + (\bar{\sigma} - \sigma_l)\frac{\omega[\exp(\lambda l) - 1]}{1 + \omega[\exp(\lambda l) - 1]} \approx \sigma_l + (\bar{\sigma} - \sigma_l)[1 - \exp(-\lambda l)] \quad (26)$$

Once the partial debond stress, σ_d^p, has been determined using Equation 25, σ_l can be obtained by evaluating Equation 26 with respect to the debond length, l, for a given embedded fibre length, L. Therefore, the frictionless (initial) debond stress, σ_0, is determined for an infinitesimal debond length (i.e. $l \to 0$) and the maximum debond stress, σ_d^*, determined at load instability [1, 12] of the partial debond stress, σ_d^p. Further, the solution for the initial frictional pull-out stress, σ_{fr}, after complete debonding can be obtained when the debond length, l, reaches the embedded length, L, and the crack tip debond stress, σ_l, is zero. Thus

$$\sigma_{fr} = \frac{\omega\bar{\sigma}[\exp(\lambda L) - 1]}{1 + \omega[\exp(\lambda L) - 1]} \approx \bar{\sigma}[1 - \exp(-\lambda L)] \quad (27)$$

It is worth noting here that the solution for the partial debond stress, σ_d^p, of Equation 26 is similar to those obtained in the Gao–Mai–Cotterell [2] or Hsueh's model [4] in which σ_d^p is composed of two components: a crack tip debond stress, σ_l, and a friction stress component. The second component is directly proportional to $(\bar{\sigma} - \sigma_l)$ and is also controlled by λ (or coefficient of friction at the interface, μ). However, there is an obvious difference in the crack tip debond stress, σ_l, which is not only a function of the interfacial fracture toughness, G_{ic}, but is also dependent on the debond length, l, relative to the total embedded fibre length, L, in this new model. In contrast, in Gao *et al.*'s model [2], σ_l is invariant with l or L and it depends only on G_{ic}, while in Hsueh's model [3, 4] it is controlled by the shear bond strength, τ_b, at the interface (instead of G_{ic}) and is constant for a given remaining bond length regardless of whether there is partial debonding or not. Therefore, in the previous two theories, the crack tip debond stress, σ_l, is considered to be equal to the frictionless (initial) debond stress, σ_0, for an identical remaining bond length. Further details on the differences between σ_l and σ_0 will be discussed in Section 4. Apart from the partial debond stress, σ_d^p, the post-debond frictional pull-out stress, σ_{fr}, obtained in the present analysis is basically identical to those obtained in previous models if $\omega \to 1$ (i.e. $b \gg a$) which is common in practical fibre pull-out experiments.

3. Results

Single-fibre pull-out tests were performed on composite systems of (both untreated and electrolytically oxidized) carbon fibre–epoxy matrix ($a = 0.003$ mm and $b = 1.0$ mm) and (both uncoated and release-agent coated) stainless steel wire–epoxy matrix ($a = 0.275$ mm and $b = 6.5$ mm). Published data for a (both untreated and acid treated) SiC fibre–borosilicate glass matrix composite ($a = 0.071$ mm and $b = 2.8$ mm) [13] are also used to compare with theoretical predictions. In Part I of this paper [1], the interfacial properties for these composite systems were determined by evaluating experimental results with regard to the asymptotic debond stress, $\bar{\sigma}$, and the reciprocal friction length, λ, and are summarized along with other material constants in Table I. Although slight improvement in the interfacial bond strength is observed for some electrolytically oxidized carbon fibres, for simplicity they are treated in the same data group as the untreated fibres with identical properties in Table I. Using these properties, specific results of the partial debond stress, σ_d^p, are calculated as a function of debond length, l, with respect to total embedded fibre length, L, from which instability conditions are identified. The maximum debond stresses, σ_d^*, determined at instability are compared with experimental results. At these maximum debond stresses, σ_d^*, the corresponding stress distributions in the constituents are calculated for different L to show deformations in the composites during the fibre pull-out process. The implications of the stress distributions for different composite systems on the debond

TABLE I Mechanical properties of constituents and interfacial properties for different fibre composites

Composite system	Fibre surface condition	Properties of fibre and matrix				Interfacial properties			
		E_f (GPa)	E_m (GPa)	ν_f	ν_m	G_{ic} (Jm^{-2})	μ	q_0 (MPa)	z_{max} (mm)
Carbon fibre–epoxy matrix	Untreated and oxidized	230	3.0	0.2	0.4	37.7	1.25	− 9.97	0.145
Steel wire–epoxy matrix	Uncoated	179	2.98	0.3	0.35	1316	0.48	− 8.85	12.0
	Release-agent coated	179	2.98	0.3	0.35	34.7	0.22	− 7.28	6.95
SiC fibre–glass matrix	Untreated	400	70	0.17	0.2	0.964	0.048	− 64.5	0.505
	Acid treated	400	70	0.17	0.2	2.40	0.078	− 72.3	0.485

criterion proposed in the present analysis are discussed.

3.1. Partial debond stress, σ_d^p, and instability of debond process

The partial debond stress, σ_d^p, calculated based on Equations 25 or 26 are plotted against debond length, l, as shown in Figs 2 and 3, respectively, for carbon fibre–epoxy matrix and untreated SiC fibre–glass matrix composites. These two composite systems are considered to be typical of those with fibre–matrix interface that are either chemical or frictional in nature. In general, for a given total embedded fibre length, L, as debond length, l, increases the friction stress component increases steadily, the increase being non-uniform due to Poisson contraction of the fibre in the debonded region. However, the crack tip debond stress, σ_l, decreases towards zero depending on L. The instability criterion developed by the authors [12] requires that the derivative of the partial debond stress with respect to the remaining bond length $(L - l)$ is equal to or less than zero. This means that the debond process becomes unstable if $(L - l)$ is smaller than z_{max} (shown in Fig. 2) where the maximum debond stress, σ_d^*, is obtained. Further, if the total embedded fibre length, L, is even smaller than z_{max} (e.g.

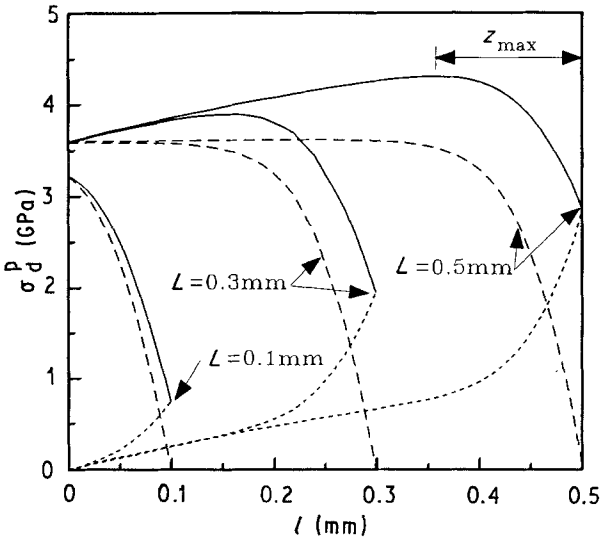

Figure 2 Plots of partial debond stress, σ_d^p, as a function of debond length, l, calculated based on Equation 25 or 26 at different embedded fibre length, L, for carbon fibre–epoxy matrix composites: (——) partial debond stress, σ_d^p, (– – –) crack tip debond stress, σ_l; (- - -) friction stress component.

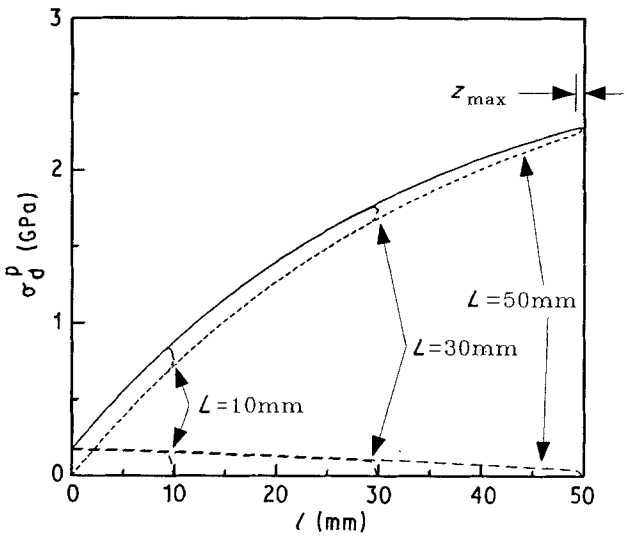

Figure 3 Plots of partial debond stress, σ_d^p, as a function of debond length, l, calculated based on Equation 25 or 26 at different embedded fibre lengths for untreated SiC fibre–borosilicate glass matrix composites. Symbols as in Fig. 2.

L = 0.1 mm in Fig. 2), the debond process is unstable from the beginning without any partial debonding. In this case, σ_d^* is determined simply when the debond crack initiates (which is the frictionless initial debond stress, σ_0). In other words, the contribution of friction stress component to σ_d^* becomes increasingly important as L increases. The importance of friction at the debonded region, which in turn determines the stability of the debond process, is also very much dependent on the nature of bonding at the interface (which can be expressed by the interfacial fracture toughness, G_{ic}, or shear bond strength, τ_b, compared to the frictional shear stress). For example, the contribution of friction stress component to σ_d^* is merely 20% at L = 0.5 mm for the carbon fibre–epoxy matrix composite in Fig. 2 (which is typical of good chemical bonding at the fibre–matrix interface), while it is more than 95% at L = 50 mm for the untreated SiC fibre–glass matrix composite in Fig. 3 (which is typical of principally frictional bonding at the interface). This interfacial property-dependent debonding process is reflected by the amount of load drop (i.e. from the maximum debond stress, σ_d^*, to a lower value corresponding to the initial frictional pull-out at $L = l$) in Figs 2 and 3 which resembles the load drop frequently observed in pull-out stress versus displacement curves in the experiments. Therefore, in Part I of this paper [1] three different interfacial debond processes were identified

in terms of the maximum bond length, z_{max}, below which the debond process becomes unstable. It follows that, depending on the debond length, l, relative to the total embedded fibre length L, σ_d^p is classified into the frictionless (initial) debond stress σ_0 at $l = 0$, the maximum debond stress σ_d^* at $l = L - z_{max}$ (or $l = 0$ if $L < z_{max}$), and the initial frictional pull-out stress, σ_{fr}, after complete debonding at $l = L$. z_{max} values for different composite systems determined in the present analysis are given in Table I which are comparable to those obtained by using Hsueh's model as reported in Part I of this paper [1]. It should be reiterated here that the original Gao–Mai–Cotterell model [2] predicts progressive stable debonding because σ_d^p always increases with l at the same rate as the friction stress component. Therefore, σ_d^* is obtained always at the moment of complete debonding when $l = L$ and the model is not able to evaluate the instability condition during progressive debonding.

3.2. Comparison of maximum debond stress, σ_d^*, between theories and experiments

The maximum debond stress, σ_d^*, determined at instability of the partial debond stress, σ_d^p, are compared with experimental results for three composite systems as shown in Fig. 4. Also superimposed are the predictions by the Gao *et al.* model [2] (based on Equation 9 in Reference 1). Because the solutions for the post-debond frictional pull-out stress obtained in the present analysis are basically the same as the previous model [2] which shows excellent agreement with experimental results for all composite systems compared, the specific results are not presented here. Very good agreement is obtained between the present analysis and the experimental results over the whole range of L and for all composites studied. A major improvement of the present analysis over the previous model is its capability of accurate prediction for small L where the Gao *et al.*'s model always overestimates and gives a finite value at $L = 0$ due to the assumed constant crack tip debond stress, σ_l (or frictionless initial debond stress, σ_0, in this case). This is particularly true for epoxy-based matrix composites (Fig. 4a and b) having good chemical bonding at the interface.

3.3. Stress distributions in the constituents

The stress distributions in the constituents calculated along the z-direction by using Equations 9, 10 and 12 in the bonded region ($l \leqslant z \leqslant L$) and Equations 16, 17 and 21 in the debonded region ($0 \leqslant z \leqslant l$) are shown in Figs 5 and 6 for the carbon fibre–epoxy matrix and untreated SiC fibre–glass matrix composites. The external stress applied to the free fibre-end for each embedded fibre length is the maximum debond stress, σ_d^*, given in Fig. 4. For this reason, the stress distributions are shown only at the bonded region for the carbon fibre–epoxy matrix composite with $L = 0.1$ mm in Fig. 5. For the carbon fibre–epoxy matrix composites, the stress gradients for all these stress distributions increase (or decrease in the case of the axial matrix stress shown in Fig. 5b) rapidly from the matrix bottom (i.e. $L - z = 0$) to the boundary

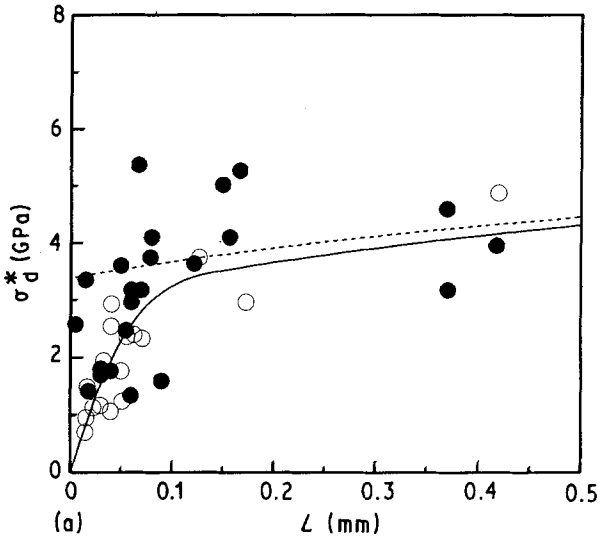

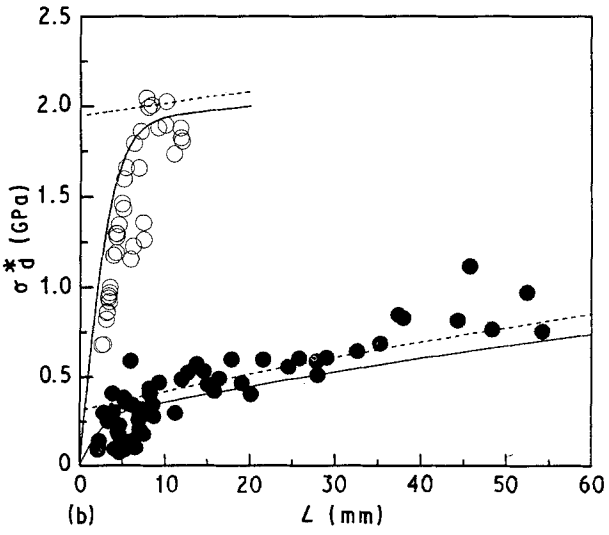

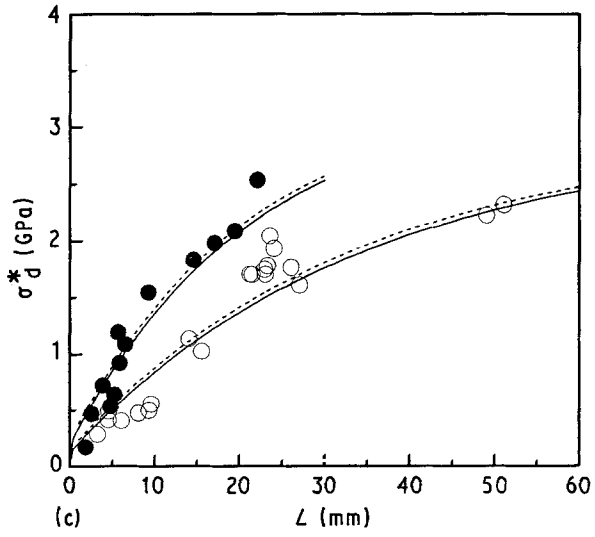

Figure 4 Comparisons between experimental results and theoretical predictions of maximum debond stress, σ_d^*, as a function of embedded fibre length L for (a) (○) untreated and (●) oxidized carbon fibre–epoxy matrix composites, (b) (○) uncoated and (●) release-agent coated steel wire–epoxy matrix composites and (c) (○) untreated and (●) acid treated SiC fibre–glass matrix composites. Predictions: (——) present analysis; (– – –) Gao *et al.* [2].

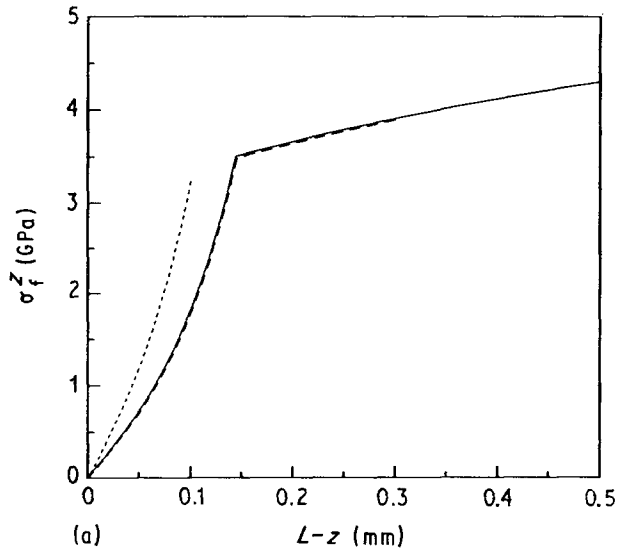

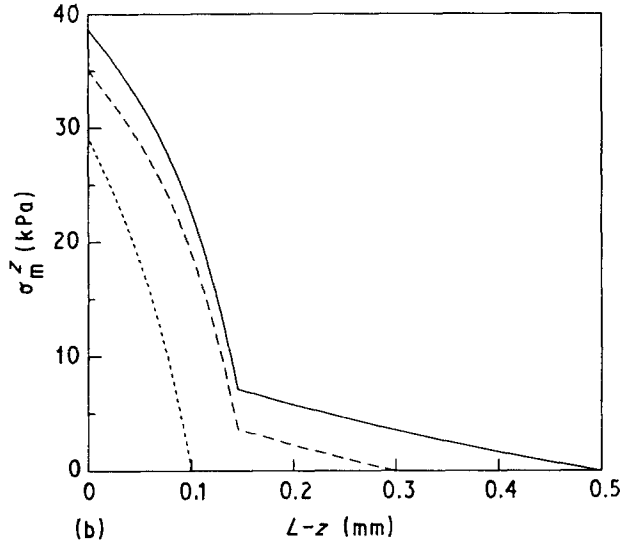

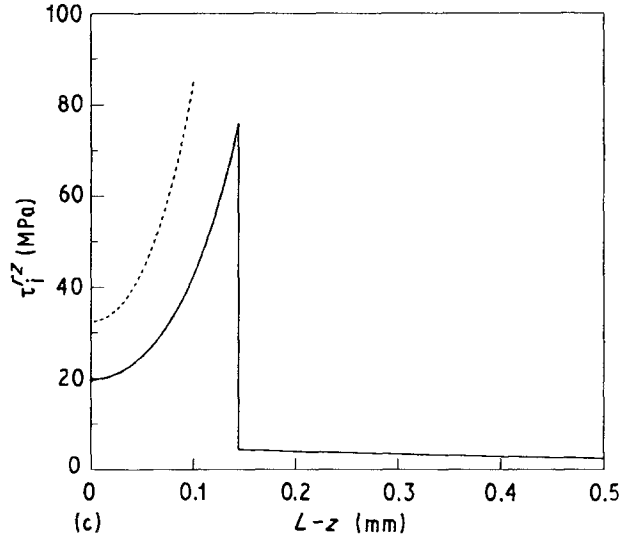

Figure 5 Distributions of (a) fibre axial stress, σ_f^z, (b) matrix axial stress, σ_m^z, and (c) interfacial shear stress, τ_i^{rz}, along the fibre length $(L - z)$ for carbon fibre–epoxy matrix composite at maximum debond stress, σ_d^*: (- - -) $L = 0.1$ mm; (– – –) $L = 0.3$ mm; (——) $L = 0.5$ mm.

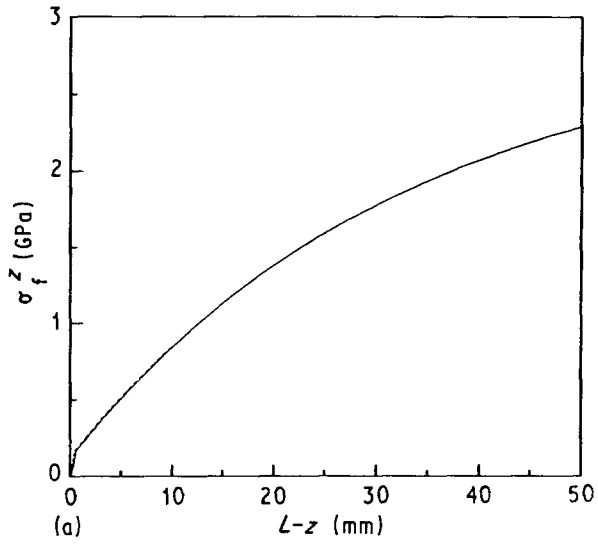

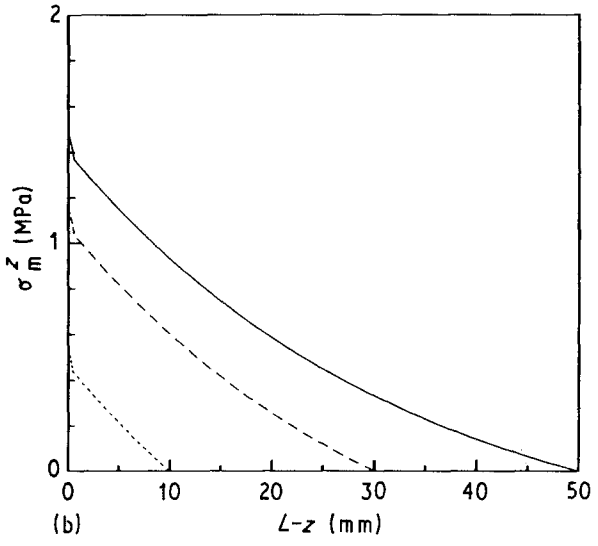

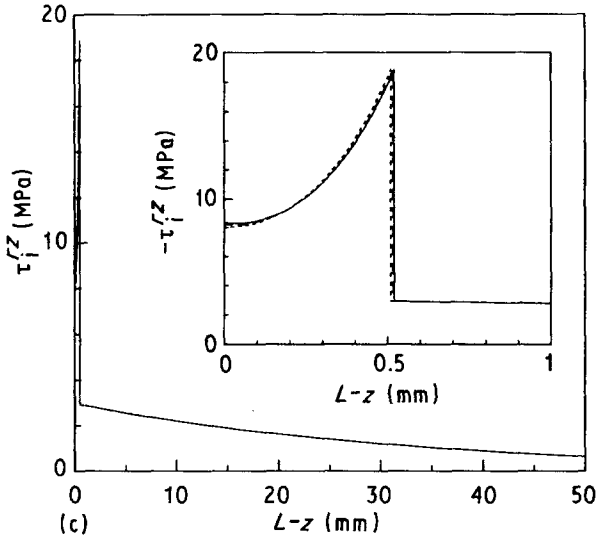

Figure 6 Distributions of (a) fibre axial stress, σ_f^z, (b) matrix axial stress, σ_m^z, and (c) interfacial shear stress, τ_i^{rz}, along the fibre length for untreated SiC fibre–borosilicate glass matrix composites at maximum debond stress, σ_d^*: (- - -) $L = 10$ mm; (– – –) $L = 30$ mm; (——) $L = 50$ mm.

between bonded and debonded regions (i.e. at the debond crack tip, $L - z = z_{max}$), and become almost constant at the debonded region. The same observation holds for the untreated SiC fibre–glass matrix composites (Fig. 6), although the stress distributions in the bonded regions are rather unclear due to the very small z_{max} value relative to the allowable embedded fibre length, L. The high level of stress concentration near the debond crack tip (or near the free fibre-end if $L < z_{max}$), particularly the interfacial shear

stress, is a direct reflection of the imminent unstable debond crack propagation as the applied fibre stresses are σ_d^*. It is interesting to note that for both systems if $L \geqslant z_{max}$, the stress distributions of the axial fibre and interfacial shear stresses (Figs 5a, c, 6a and c) are almost identical independent of L, especially in the debonded region. However, this observation does not apply to the matrix axial stress (Figs 5b and 6b). This seems to be attributed to the assumption that average values are taken for the matrix axial stress with respect to the radial direction as in Equation 6. Unlike the axial stresses in the fibre and matrix, the interfacial shear stress distributions are discontinuous at the boundary between bonded and debonded regions. In the debonded region, the interfacial (frictional) shear stress decreases toward zero near the fibre free end due to the Poisson contraction of the fibre in the radial direction. If embedded fibre length, L, is further increased, σ_d^* shown in Fig. 4 would increase to a critical (plateau) value, $\bar{\sigma}$, such that the induced radial (tensile) stress at the interface compensates completely the residual clamping (compressive) stress arising from matrix shrinkage (i.e. $q_0 + q^*(z) = 0$ in Equation 15) and the corresponding interfacial (frictional) shear stress equals zero. Under this circumstance, complete separation of the frictionally bonded interface between the fibre and matrix occurs at the free surface ($z = 0$) and extends along the debonded interface.

The maximum interfacial shear stresses obtained at the end of the bonded region ($L - z = z_{max}$) are found to vary depending on the composite systems and embedded fibre length, L, while the interfacial (frictional) shear stress at the discontinuity is almost constant for a given composite system independent of L (Figs 5c and 6c). This is expected because two distinct assumptions were made for the respective regions, namely perfect interfacial bonding (Equation A3) in the bonded region and frictional slipping according to Coulomb friction law (Equation 15) in the debonded region. The stress difference at the discontinuity for the carbon fibre–epoxy matrix composite (approximately 95% the maximum value, Fig. 5c) is slightly larger than the untreated SiC fibre–glass matrix composite (about 82% of the maximum value, Fig. 6c) probably due to the difference in the nature of bonding at the interface (i.e. strong chemical bonding for the former and mechanical bonding for the latter). Both fibre composites show a significant stress gradient in the bonded region near the debond crack tip. In fact, a singular stress field has been reported previously [14, 15] based on elastic stress analysis. In a study of the microbond model of Kevlar fibre–epoxy matrix system using a finite element analysis [14], it is shown that the interfacial shear stress distribution converges asymptotically to an infinite value near (i.e. approximately 10 μm from) the loading point (which corresponds to the free fibre-end in the present model), depending on the specimen shape and dimensions. A similar conclusion has also been reached for a fibre pull-out model of a glass rod–polyurethane matrix system using both analytical and numerical methods [15]. In reality, of course, the critical interfacial shear stress must have a finite value at debonding.

The functional dependence of the shear stress in the bonded region on L can be further studied in a plot of the maximum interfacial shear stresses versus L as shown in Fig. 7 for the carbon fibre–epoxy matrix and SiC fibre–glass matrix composites. The applied stress is σ_d^* given in Fig. 4. It is found that if $L < z_{max}$ the maximum interfacial shear stress $\tau_{i(max)}$ increases systematically towards a certain finite value as L decreases to zero, while it gives a constant value if $L \geqslant z_{max}$. An almost identical result can be obtained if the applied stress is taken at initial debonding. The constant value $\tau_{i(max)} = 75.8$ MPa for $L \geqslant z_{max}$ (Fig. 7a) is slightly higher than the maximum bond strength in shear $\tau_b = 72.7$ MPa determined from the initial slope of the experimental maximum debond stress–embedded fibre length ($\sigma_d^* - L$) curves [1] for the carbon fibre–epoxy matrix system. This implies that the debond criterion proposed in the present fracture analysis predicts virtually the same level of interfacial shear stress for debond crack propagation as for the shear strength criterion if the total embedded fibre length L is longer than z_{max}. It should be

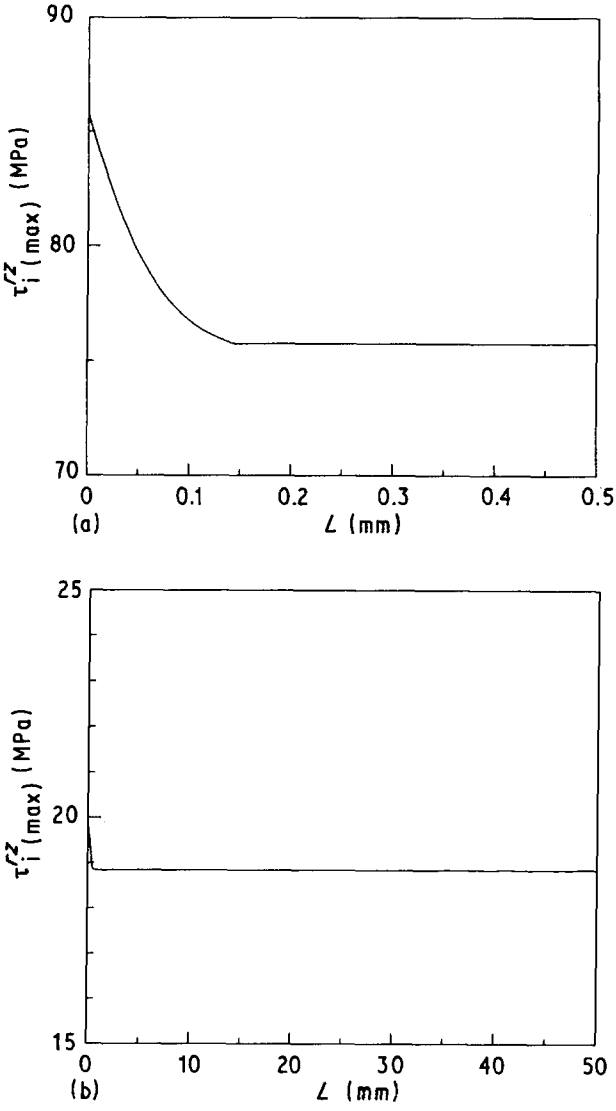

Figure 7 Plots of maximum interfacial shear stress, $\tau_{i(max)}^{rz}$, determined at the fibre free end ($L < z_{max}$) or at the debond crack tip ($L \geqslant z_{max}$) as a function of embedded fibre length, L, when the external applied stress is the maximum debond stress, σ_d^*, for (a) carbon fibre–epoxy matrix composite, and (b) SiC fibre–glass matrix composite.

mentioned here that the shear strength criterion assumes that the debond crack propagates when the interfacial shear stress reaches the maximum bond strength, τ_b, which is a material constant. However, if L is shorter than z_{max} where the debond process is totally unstable, the present model predicts that the debond process is governed primarily by the energy criterion being satisfied and a high shear stress concentration at the debond crack tip. In this case, a model based on a shear strength criterion cannot explain the observed high shear stress concentration. In other words, a constant interfacial fracture energy criterion applies and the shear stress at fracture is not a constant material property. It is noted that for the SiC fibre–glass matrix composite the maximum interfacial shear stress ($\geqslant$ 18.85 MPa, Fig. 7b) is higher by almost six times than that taken from the experimental curve (3.18 MPa [1]). This suggests that the present model based on a fracture mechanics approach inherently predicts large shear stress concentration for crack propagation even for a system which is typical of frictional bonding at the interface.

4. Discussion

A major improvement of the present model relative to the earlier Gao–Mai–Cotterell [2] model which is also based on a fracture mechanics approach is that it can predict accurately the maximum debond stress, σ_d^*, for all composite systems studied over the whole range of embedded fibre length, L, including the very short L. The Gao–Mai–Cotterell model overestimates σ_d^* for short L, giving a finite value for $L = 0$. This difference arises basically from the consideration of the elastic strain energy stored in the bonded region of the constituents as well as the matrix shear strain energy for fracture analysis of the debond criterion proposed in the present model. These strain energies are omitted in the previous model. Therefore, the present model predicts that although the frictionless (initial) debond stress, σ_0, is determined by the interfacial fracture toughness, G_{ic}, the crack tip debond stress, σ_l, acting at the boundary between bonded and debonded region during progressive debonding is not only a function of G_{ic} but also varies with partial debond length, l, relative to the total embedded fibre length, L. This enables the evaluation of the instability condition (by using the plot of the partial debond stress, σ_d^p, versus debond length, l) leading to unstable debonding at $(L - l) = z_{max}$ where σ_d^* is obtained. In the Gao–Mai–Cotterell model [2], σ_0 (or σ_l) is always constant independent of l or L, and consequently σ_d^* is obtained when the debond crack reaches the embedded fibre end (i.e. $l = L$) where the frictional stress component is the maximum. Consequently, instability condition cannot be evaluated.

In the present model, for a given bond length, the crack tip debond stress, σ_l, is different from the frictionless (initial) debond stress, σ_0. In contrast, in the Gao–Mai–Cotterell [2] and Hsueh [3.4] models, σ_l is assumed constant for an identical bond length independent of partial debond length, l, and is thus equal to σ_0 as mentioned before. This difference is schematically illustrated in Fig. 8 showing the axial stresses in the constituents on the external surface as well as on the plane corresponding to the debond crack tip for a given bond length (i.e. $L_1 = L_2 - l$). For the model in Fig. 8a, the external applied stress is the initial debond stress, σ_0, and there is a stress-free condition for the matrix top surface. However, during progressive debonding for the identical bond length (Fig. 8b), there will be a substantial stress acting on the plane of the crack tip inside the matrix which gives rise to a high corresponding fibre stress, σ_l. In Fig. 9, predicted σ_0 and σ_l values for the situations shown in Fig. 8a and b, respectively, are plotted as a function of bond length for the SiC fibre–glass matrix composite. In order to show clearly the difference, the debond lengths are assumed to be the same as the bond length (i.e. $L_2 = 2l$) for the calculation of σ_l. Also superimposed is the result of σ_0 predicted based on the Gao–Mai–Cotterell model [2]. It can be noted that σ_l is substantially larger than σ_0 even when there is small

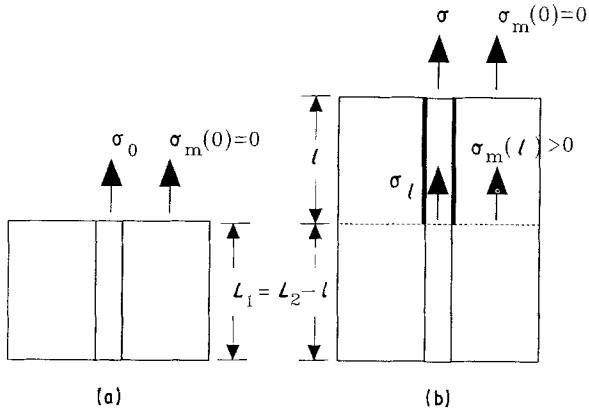

Figure 8 Schematic drawings of the fibre pull-out model for (a) initial debonding, and (b) progressive debonding showing the axial stresses in the fibre, σ_f^z, and matrix, σ_m^z, on the surface and on the plane of debond crack tip for an identical bond length.

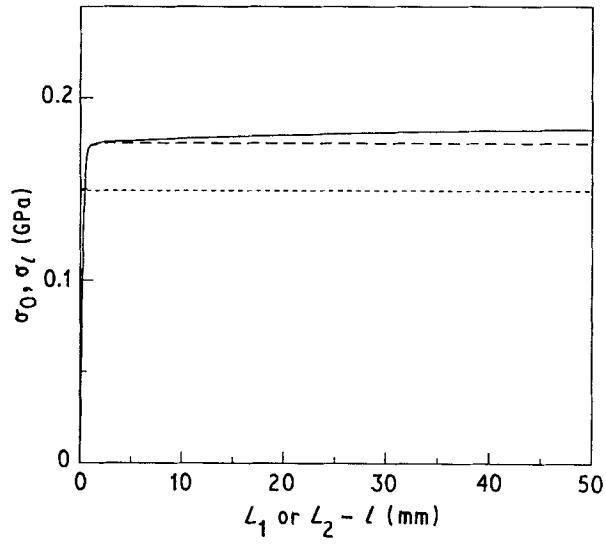

Figure 9 Comparisons of (– – –) the frictionless (initial) debond stress, σ_0, and (——) the crack tip debond stress, σ_l, as a function of the bond length, L_1 or $(L_2 - l)$ (see Fig. 8) for SiC fibre–glass matrix composite. Debond length, l, for calculation of σ_l is the same as the bond length $L_2 - l$. Also superimposed is the frictionless (initial) debond stress, σ_0 (- - -), calculated using the Gao *et al.* [2] model.

debond length and the difference increases as debond length increases. Both σ_l and σ_0 calculated based on the present model are even larger than σ_0 predicted by the Gao–Mai–Cotterell model [2]. It is also found that the difference is larger for the ceramic matrix composite than for epoxy-based matrix systems, suggesting that the difference arises mainly from contribution of stresses in the debonded region.

The evaluation of whether the interfacial debonding in a single-fibre pull-out model is fracture energy-governed or shear strength-governed, is of great interest among researchers. Leung and Li [16] have suggested that if there is a large transition zone at the debond crack tip when the material nearby breaks down (e.g. large-scale yielding of matrix material), the singularity of stress field is significantly impaired. Under this circumstance, the shear strength-based approach is more appropriate than the fracture energy-based approach, and vice versa. Leung and Li [16] proposed that it is possible to evaluate which approach is more appropriate by using a unified form of an approximate equation which is the ratio of σ_d^* to σ_{fr} as

$$\frac{\sigma_d^*}{\sigma_{fr}} = 1 + \frac{[(Y^2 - Y)]^{1/2} - \cosh^{-1} Y^{1/2}}{\beta L} \quad (28)$$

where

$$\beta = \left\{ \frac{1 + \alpha/\gamma}{(1 + \nu_m)(b^{*2} - a^2)\log(b^*/a)} \right\}^{1/2} \quad (29)$$

Equation 29 is essentially the same as Equation 5b in [1] except the effective matrix radius, b^*, (where all the axial and shear deformation is concentrated near the fibre [17]) in place of the matrix outermost radius, b. Using Equation 28 in conjunction with experimental fibre pull-out results for different fibre radii or different fibre volume fractions, Leung and Li [16] argued that if Y is constant with respect to β, debonding is shear strength-governed and Y is equal to the ratio of shear bond strength to the frictional shear strength (τ_b/τ_f) based on an approximate shear strength approach [18]. For the shear strength approach to be valid, (τ_b/τ_f) must be small (i.e. close to unity). In contrast, if Y varies with β the debonding is governed by a single fracture parameter, G_{ic} and Y can be determined according to an approximate equation taken from Gao *et al.* [2]

$$Y \approx 0.5 + (0.25 + X)^{1/2} \quad (30)$$

where

$$X = aE_f G_{ic} \beta^2/\tau_f^2 \quad (31)$$

Practical application of the foregoing argument is limited by the usually large scatter obtained for the fibre pull-out experimental results. Another important criticism of Equations 28–31 is the oversimplification of the original solutions for σ_d^* and σ_{fr} to fit into a unified equation, particularly the assumption of constant frictional shear strength, τ_f, independent of L without taking into account the effect of Poisson contraction in the debonded region.

The conditions for validity of the two different approaches are very complicated and there is no clear evidence reported hitherto. Therefore, it seems that one cannot judge the validity of one approach by a single parameter such as fibre radius even if the other properties are known. Particularly, because the interfacial properties such as the interfacial fracture toughness, G_{ic}, or the shear bond strength, τ_b, residual clamping stress, q_0, the coefficient of friction at the interface, μ, and even the interfacial frictional shear strength, τ_f, are extremely hard to determine independently with any accuracy in experiments, these properties are always varied to make the theoretical predictions fit the experimental data. Therefore, argument of good or poor agreement of maximum debond stress, σ_d^*, and the initial frictional pull-out stress, σ_{fr}, between theory and experimental results cannot give any indication that one approach is more appropriate than the other. Moreover, due to the difficulties in obtaining the actual stress field at the interface, one cannot ascertain how much the stress distributions predicted by using a model resemble the reality. In fact, the energy release rate for an incremental debond crack propagation based on a fracture mechanics approach is again insensitive to the local shear stress distribution at the interface of zero thickness. Generally speaking, a fracture mechanics approach deals with a more fundamental problem of microscopic material behaviour for a given loading configuration than a shear strength-based approach. For example, the condition for unstable debonding for a given composite with $L < z_{max}$ or $(L - l) < z_{max}$ can be better explained in terms of fracture mechanics concepts where the total energy stored in the system exceeds the energy required for debonding the whole of the remaining bonded interface. However, although a shear strength-based approach also provides a mathematical solution for z_{max}, it cannot explain the physical significance of instability of the debond process; because it assumes that debond crack propagation occurs when the interfacial shear stress exceeds the shear bond strength, τ_b, regardless of whether the subsequent debond process is stable or unstable. Because of these latter two comments, the authors believe that a model based on the fracture mechanics approach is physically more appealing than one based on the shear strength criterion.

5. Conclusion

An improved analysis of interfacial debond and frictional pull-out stresses in a fibre pull-out model is developed on the basis of the concept of fracture mechanics. The elastic strain energies stored in the fibre and matrix at both bonded and debonded regions are calculated using axial and shear stress components in a shear lag model. The differential energy with respect to incremental debond length is equated to the interfacial fracture toughness, G_{ic}, to derive the debond criterion. The partial debond stress, σ_d^p, obtained in the present analysis consists of two stress components, namely the crack tip debond stress, σ_l, at the bonded region and the friction stress component

at the debonded region, σ_l is not only a complex function of the elastic constants of the constituents, interfacial properties and geometry factors, but is also dependent on the debond length, l, relative to the total embedded length, L. Therefore, the present model is able to evaluate the instability condition where the maximum debond stress, σ_d^*, is determined. This is in sharp contrast to the result of a previous analysis by Gao *et al.* [2] based on a similar fracture mechanics approach, that σ_l is constant and independent of l or L so that σ_d^* is always obtained at complete debonding. Comparisons between theory and experimental fibre pull-out results on several composite systems including carbon fibre–epoxy matrix, stainless steel wire–epoxy matrix, SiC fibre–glass matrix show that the present model predicts excellently the maximum debond stress, σ_d^*, for all composite systems over a wide range of L, including even the very short L (whereas the previous model overestimates σ_d^* and gives a finite value for $L = 0$). The initial frictional pull-out stress, σ_{fr}, after complete debonding predicted by the present model is basically the same as the previous model, both of which agree well with experimental data.

Acknowledgements

The authors thank the Australian Research Council (ARC) for continuing support of this work which forms part of a larger project on "Development of High Strength and High Fracture Toughness Composites with Controlled Interfaces". They also thank B. Cotterell for many useful suggestions and stimulating discussions. Experimental data for the carbon fibre–epoxy matrix composites were provided by courtesy of C. Baillie, University of Surrey, UK. L.M.Z. is supported by a University of Sydney Postgraduate Research Scholarship and J.K.K. by an Australian Postgraduate Research Award, a P. N. Russell Scholarship and an ARC Junior Research Fellowship.

Appendix 1. Stress transfer in the bonded region ($l \leqslant z \leqslant L$)

When the fibre is subjected to a tensile stress, σ, the stress is transferred from the fibre to the matrix through the interfacial shear stress, $\tau_i^{rz}(z)$, such that the equilibrium condition can be obtained by combining Equations 7 and 8 as

$$\frac{d\sigma_m^z(z)}{dz} = \frac{2\gamma}{a}\tau_i^{rz}(z) \tag{A1}$$

To satisfy the equilibrium condition between the axial and shear stresses in the cylindrical shell of matrix, we have

$$\frac{\partial\sigma_m^z(z)}{\partial z} + \frac{\partial\tau_m^{rz}(r, z)}{\partial r} + \frac{\tau_m^{rz}(r, z)}{r} = 0 \tag{A2}$$

Therefore, the shear stress in the matrix, $\tau_m^{rz}(r, z)$, can be expressed as a function of the interfacial shear stress, $\tau_i^{rz}(z)$, for the boundary conditions that the stresses are compatible at the interface (i.e. $\tau_m^{rz}(a, z) = \tau_i^{rz}(z)$) and the stress is free at the matrix cylindrical surface (i.e. $\tau_m^{rz}(b, z) = 0$)

$$\tau_m^{rz}(r, z) = \frac{\gamma(b^2 - r^2)}{ar}\tau_i^{rz}(z) \tag{A3}$$

Combining Equations 5 and A3 for the boundary condition of axial displacement continuity at the bonded interface (i.e. $u_m^z(a, z) = u_f^z(a, z)$) and differentiation with respect to z gives

$$\frac{d\tau_i^{rz}(z)}{dz} = \frac{aE_m[\varepsilon_m^z(b, z) - \varepsilon_f^z(a, z)]}{(1 + \nu_m)[2\gamma b^2 \ln(b/a) - a^2]} \tag{A4}$$

where the relations between the stress components and the axial strains in the constituents ε_f^z and ε_m^z are given in Equations 1 and 3. The condition that the fibre and the matrix remain in contact during deformation requires continuity of tangential strain (or radial displacement) at the interface (i.e. $\varepsilon_f^\theta(a, z) = \varepsilon_m^\theta(a, z)$ given in Equations 2 and 4) such that [2]

$$q^* = \frac{\alpha\nu_f\sigma_f^z(z) - \nu_m\sigma_m^z(z)}{\alpha(1 - \nu_f) + 1 + \nu_m + 2\gamma} \tag{A5}$$

where $q^*(= \sigma_f^r(a, z) = \sigma_m^r(a, z))$ is the radial stress at the interface caused by Poisson contraction of the fibre which is subjected to tensile stress. Gao *et al.* [2] previously obtained Equation A5 by considering a thin fibre (i.e. $\sigma_f^r(z) = \sigma_f^\theta(z)$) and a plane strain deformation of the matrix with a stress free cylindrical surface in the radial direction (i.e. $\sigma_m^\theta(b, z) = -2\gamma\sigma_m^r(a, z)$ and $\sigma_m^r(b, z) = 0$). Combining Equations 1, 3, 7, A4 and A5 yields a differential equation for the axial fibre stress $\sigma_f^z(z)$ as

$$\frac{d^2\sigma_f^z(z)}{dz^2} - A_1\sigma_f^z(z) = A_2\sigma \tag{A6}$$

where the coefficients A_1 and A_2 are functions of the elastic properties and geometric factors of the constituents and are given in Equations 13 and 14. The solution of $\sigma_f^z(z)$ is subjected to the following boundary conditions

$$\sigma_f^z(l) = \sigma_l = \sigma - \omega(\bar{\sigma} - \sigma)[\exp(\lambda l) - 1] \tag{A7}$$

$$\sigma_f^z(L) = 0 \tag{A8}$$

In Equation A7, σ_l is defined as the crack tip debond stress at the boundary between the bonded and debonded regions at $z = l$ where the axial fibre stress given in Equation 16 must be continuous. From the solution of fibre axial stress, $\sigma_f^z(z)$, as given in Equation 9, the corresponding matrix axial stress, $\sigma_m^z(z)$, and shear stresses in the matrix, $\tau_m^{rz}(z)$, and the interface $\tau_i^{rz}(z)$ are obtained in Equations 10–12, respectively.

Appendix 2. Coefficients *B*, *C* and *D*

$$\begin{aligned} B = {} & \{n_2 - \Phi(n_2 - n_1A_1)[1 + (A_2/A_1) \\ & \times(1 + A_2/A_1)(2 - 2\cosh\Phi + \tanh\Phi \\ & \times\sinh\Phi)]\coth\Phi + [2n_2(A_2/A_1) \\ & \times(1 + A_2/A_1) - n_3(1 + 2A_2/A_1)] \\ & \times(1 - \cosh\Phi)\}\operatorname{cosech}^2\Phi - n_4 \end{aligned} \tag{A9}$$

$$\begin{aligned} C = {} & \omega\exp(\lambda l)\{\lambda H + [dH/dl - \pi a^2/E_f] \\ & \times[1 - \exp(-\lambda l)]\} \end{aligned} \tag{A10}$$

$$D = \omega^2\exp(2\lambda l)\{[1 - \exp(-\lambda l)]\{(\lambda/A_1^{1/2}) \times [(n_2 + n_1A_1)\cosh\Phi \sinh\Phi - \Phi(n_2 - n_1A_1)] + [1 - \exp(-\lambda l)] \times [n_2 - \Phi(n_2 - n_1A_1)\coth\Phi]\}\operatorname{cosech}^2\Phi + n_1\lambda^2 + n_2[1 - \exp(-\lambda l)]^2\} \quad \text{(A11)}$$

where

$$\Phi = A_1^{1/2}(L - l) \quad \text{(A12)}$$

$$n_1 = \frac{\pi\gamma(1 + \nu_m)}{2E_m}\{b^4\ln(b/a) - (3b^2 + a^2)(b^2 + a^2)/4\} \quad \text{(A13)}$$

$$n_2 = \frac{\pi a^2}{2E_m}(\alpha + \gamma) \quad \text{(A14)}$$

$$n_3 = \frac{\pi a^2}{E_m}[(\alpha + \gamma)(A_2/A_1) + \gamma] \quad \text{(A15)}$$

$$n_4 = \frac{\pi a^2}{2E_m}\{\alpha[(A_2/A_1)^2 - 1] + \gamma(A_2/A_1 + 1)^2\} \quad \text{(A16)}$$

and

$$H = (1/A_1^{1/2})\{\{(1 + A_2/A_1)[(n_2 - n_1A_1) \times (1 + \Phi\operatorname{cosech}\Phi) + 2n_1A_1] - n_3\} \times (1 - \cosh\Phi) - (n_2 - n_1A_1) \times (1 - \Phi\coth\Phi) - 2n_1A_1\}\operatorname{cosech}\Phi \quad \text{(A17)}$$

References

1. J. K. KIM, C. BAILLIE and Y. W. MAI, *J. Mater. Sci.* (1991) **27**, 3143.
2. Y. C. GAO, Y. W. MAI and B. COTTERELL, *J. Appl. Math. Phys. (ZAMP)* **39** (1989) 550.
3. C. H. HSUEH, *Mater. Sci. Engng* **A130** (1990) L11.
4. *Idem., ibid.* **A123** (1990) 1.
5. M. R. PIGGOTT, *Comp. Sci. Technol.* **30** (1987) 295.
6. L. M. ZHOU, J. K. KIM and Y. W. MAI, *ibid.* (1991) in press.
7. J. W. HUTCHINSON and H. M. JENSEN, *Mech. Mater.* **9** (1990) 139.
8. L. B. FREUND, *Eur. J. Mech. A.* (1991) in press.
9. L. N. McCARTNEY, *Proc. R. Soc. Lond.* **A425** (1989) 215.
10. J. K. KIM and Y. W. MAI, *Comp. Sci. Technol.* **11** (1991) 333.
11. L. S. PENN and S. M. LEE, *J. Comp. Tech. Res. (JCTRER)* **11** (1989), 23.
12. J. K. KIM, C. BAILLIE and Y. W. MAI, *Scripta Metall. Mater.* **25** (1991) 315.
13. E. P. BUTLER, E. R. FULLER Jr and H. M. CHAN, *Mater. Res. Soc. Symp. Proc.* **170** (1990) 17.
14. H. F. WU and C. M. CLAYPOOL, *J. Mater. Sci. Lett.* **10** (1991) 260.
15. C. ATKINSON, J. AVILA, E. BETZ and R. E. SMELSER, *J. Mech. Phys. Solids* **30** (1982) 97.
16. C. K. Y. LEUNG and V. C. LI, *J. Mater. Sci. Lett.* (1991) in **9** (1990) 1140
17. B. BUDIANSKY, J. W. HUTCHINSON and A. G. EVANS, *J. Mech. Phys. Solids* **34** (1986) 167.
18. C. K. Y. LEUNG and V. C. LI, *Composites* **21** (1990) 305.

Received 20 September
and accepted 26 September 1991